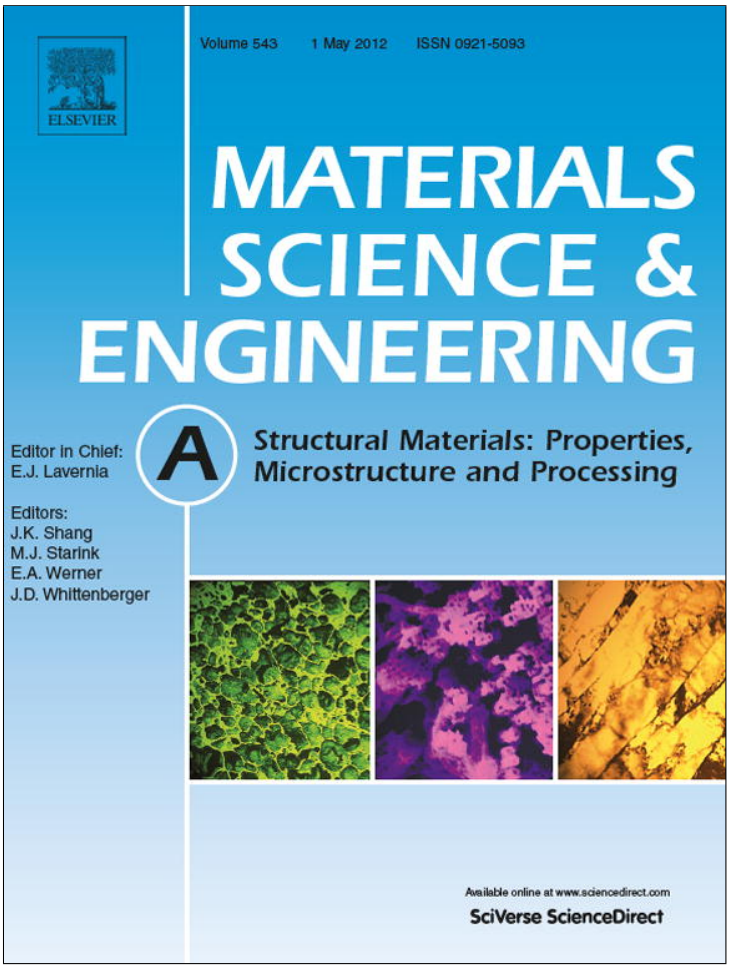

Materials Science and Engineering A 543 (2012) 88–95

Contents lists available at SciVerse ScienceDirect

Materials Science and Engineering A

journal homepage: www.elsevier.com/locate/msea

# Improvements in the mechanical properties of the 18R ↔ 6R high-hysteresis martensitic transformation by nanoprecipitates in CuZnAl alloys

Franco de Castro Bubani[a,b], Marcos Sade[a,b,c,*], Francisco Lovey[a,c]

[a] Centro Atómico Bariloche (CNEA), Av. E. Bustillo km. 9,5 (8400) S.C. de Bariloche, Argentina
[b] CONICET, Argentina
[c] Instituto Balseiro, Universidad Nacional de Cuyo, Argentina

ARTICLE INFO

*Article history:*
Received 9 January 2012
Received in revised form 16 February 2012
Accepted 17 February 2012
Available online 28 February 2012

*Keywords:*
Shape-memory alloys
Mechanical characterization
Martensitic transformation
Phase transformation
Precipitation

ABSTRACT

The 18R ↔ 6R martensite–martensite transformation in Cu-based alloys exhibits large hysteresis, large pseudoelastic strain and weak transformation stress dependence on temperature. However, concomitant plastic deformation taking place in the 6R phase inhibits the use of these properties for applications. A novel approach to minimizing or even suppressing 6R plastic deformation during the 18R–6R transformation in CuZnAl shape-memory alloy single crystals with electronic concentration $e/a = 1.48$ is presented. The method is based on a thermal treatment that introduces nanoprecipitates in the alloy. Results suggest that the role of CuZnAl shape-memory alloys in engineering should be reconsidered, as many energy damping applications could benefit from the huge hysteresis associated with the 18R–6R transformation, once the 6R plastic deformation is suppressed.



## 1. Introduction

The potential application of shape-memory alloys (SMA) in damping devices for civil structures, like buildings and bridges, to smooth out the oscillations produced by earthquakes, winds, etc., has been a subject of increasing interest in recent years. The pseudoelastic effect and the hysteresis cycle associated to the martensitic transformation in SMA are used to dissipate the energy of the oscillations [1–9].

Several relevant parameters are to be considered in this kind of applications. Firstly, the hysteresis width associated to the pseudoelastic cycle. The wider the hysteresis, the larger the dissipated energy will be in each cycle, providing for a more efficient damping device. Secondly, the critical stresses to induce the pseudoelastic effect depend on the working temperature, through the Clausius–Clapeyron equation [10]. A strong variation of these stresses with temperature will change the stiffness and the resonance frequencies of structures. As a result, the performance of damping devices would also be ambient-temperature dependent. In addition, other important parameters to take into account are: the evolution of the pseudoelastic cycles during cycling, the number of cycles until fracture, the evolution of the material itself due to atom diffusion effects, with time and temperatures, etc.

So far, NiTi-based alloys have been the most extensively studied materials, using the B2 ↔ B19′ martensitic transformation as a pseudoelastic mechanism. The average hysteresis width in the first pseudoelastic pull–pull cycle ranges from about 200 MPa to about 400 MPa, depending on several factors, namely: specimen preparation method, crystallographic texture, wire diameter or specimen size, working temperature, amount of elongation, deformation velocity, etc. [5,11–15]. Ni–Ti wires textured along the $[1\,1\,1]_{\beta 2}$ direction can undergo about 9% pseudoelastic strain [15]. However, the pseudoelastic behavior degrades rapidly in the first cycles towards an asymptotic behavior. The final reasonably steady state is reached after a few hundred cycles. The average hysteresis width drops to a value which is roughly (or sometimes less than) one half of its initial value. In addition, non-recoverable strain accumulates in the material during cycling, reducing the length of the pseudoelastic deformation by an amount that could reach up to about 4% of the initial useful length [7–16], depending on the several aforementioned factors. Both effects, i.e., the reduction in hysteresis width and the reduction in pseudoelastic strain, will result in a strong reduction in damping capacity during cycling.

Another important aspect to be taken into account for the use of SMA in damping devices is related to the temperature dependence of transformation stresses ($\sigma$). In NiTi alloys, transformation stresses depend strongly on the working temperature [9,14,15]. The

* Corresponding author. Tel.: +54 2944 445265; fax: +54 2944 445290.
*E-mail addresses:* franco@cab.cnea.gov.ar (F.d.C. Bubani), sade@cab.cnea.gov.ar (M. Sade), lovey@cab.cnea.gov.ar (F. Lovey).

0921-5093/$ – see front matter © 2012 Elsevier B.V. All rights reserved.
doi:10.1016/j.msea.2012.02.051

most acceptable value given for the B2 ↔ B19′ martensitic transformation is $d\sigma/dT = 6.3$ MPa/K [14].

On the other hand, some interesting studies have also been carried out in CuAlBe alloys as applied to damping devices. The β ↔ 18R transformation in polycrystalline CuAlBe alloys has been chosen for damping prototypes of applications for civil structures, such as family houses [7,8,17]. The average hysteresis width in the tensile pseudoelastic behavior of CuAlBe polycrystalline materials ranges from about 20 to 150 MPa, depending on grain size, amount of pseudoelastic deformation, previous thermal treatments, deformation velocity, etc. The pseudoelastic behavior in CuAlBe degrades rapidly in the first cycles towards an asymptotic behavior, similarly to NiTi alloys. The final reasonably steady state is reached after about a hundred cycles. The hysteresis width reduces to a value which is roughly (or sometimes less than) half of its initial value. The pseudoelastic strain in the first cycle can be about 6.5%. However, this recoverable deformation is reduced by cycling by an amount which depends on the several factors aforementioned [7,8,14,18,19]. The best value for the relation between transformation stresses and working temperature is $d\sigma/dT = 2.2$ MPa/K [14], which is much lower than the value for NiTi given above. Very little attention has been paid to the damping capacity in other Cu-based alloys, such as CuAlNi [20,21] or CuAlMn [22], and ferrous alloys such as FeMn-based alloys [23].

In this report, we consider the 18R ↔ 6R martensite-to-martensite transformation in CuZnAl alloys. These alloys, depending on their composition, can undergo several martensitic transformations between metastable phases, which are induced either by temperature changes or by mechanical stresses [10,24–26]. In alloys with electronic concentration $e/a = 1.48$ and β ↔ 18R martensitic transformation temperature $M_s$ close to 273 K, when a single crystal is strained in tension at temperatures above $M_s$, two martensitic transformations can be observed. First, the metastable β phase, usually called austenite, transforms into the 18R martensitic phase. This transformation can be reversed, with relatively small hysteresis. However, if the sample is further strained, the 18R phase could transform into the 6R martensite, depending on the orientation of the tensile axis. The 6R martensite has an FCT-type structure [10]. This phase transition shows stress hysteresis of about 150 MPa [25,27], whereas the deformation associated to a complete 18R–6R transformation is about 10% for a completely transformed material. A noticeable fact which makes this transition extremely interesting for applications is that, starting from the β phase, a reversible deformation of up to approximately 20% can be obtained if a complete β–18R–6R transition is produced. In order to induce the 18R–6R transformation, the tensile axis must be within about 22° from the $[1\,0\,0]_\beta$ direction, otherwise the 18R phase undergoes brittle fracture without a noticeable yield point; occasionally, 2H martensite might be observed after fracture [28].

An important additional detail of this work is based on the fact that the 18R ↔ 6R transformation and retransformation stresses ($\sigma$) show weak temperature dependence. In [10,29–32], several reported values for the variation of the critical resolved shear stress with temperature $d\tau/dT$ are mentioned, ranging from −0.12 to −0.15 MPa/K. Considering the possible tensile orientations, $d\sigma/dT$ might reach an absolute value (as it is always a negative dependence) of up to 0.42 MPa/K. These values are considerably less than those found in the B2 ↔ B19′ transformation in NiTi (6.3 MPa/K) and also less than those found in the β ↔ 18R transformation in polycrystalline CuAlBe alloys (about 2.2 MPa/K), given above. The slightly negative $d\sigma/dT$ observed in the 18R–6R transformation gives the CuZnAl system unique and completely new functionality compared to conventional SMAs, as 10% pseudoelastic strain can be obtained with a stress plateau that is expected to stay almost constant in a wide range of temperatures. Therefore, the use of the 18R ↔ 6R transformation in damping devices or other applications integrated into mechanical structures would be more advantageous, as ambient temperature changes would cause variations in structure stiffness and resonant frequencies which are smaller than those obtained with other alloys. In addition, it should be remarked that the hysteresis associated with the 18R ↔ 6R transformation in CuZnAl single crystals is greater than the hysteresis observed in polycrystalline CuAlBe and comparable to the asymptotic behavior of NiTi alloys after cycling. Moreover, the 18R ↔ 6R transformation is able to recover more than 10% strain, which is somewhat greater than the recoverable β ↔ 18R strain in Cu-based alloys and the B2 ↔ B19′ strain in Ni–Ti alloys.

Previous studies [30,33] show, nevertheless, that the 6R phase in Cu–Zn–Al single crystals suffers plastic deformation while it is being formed. This fact renders the mechanical behavior irreversible, creating difficulties for possible engineering implementations of this transformation. Cuniberti and Romero studied the 18R–6R transformation in Cu–Zn–Al single crystals with electronic concentration $e/a = 1.48$ and 1.41 and found, by trace analysis, that the 6R slip systems are $\{1\,1\,1\}_{FCT}[1\,1\,0]_{FCT}$ [33]. These authors also reported a slip system whose plane is parallel to the basal plane of the 6R martensite, with a slip direction parallel to $[0\,1\,0]_{18R}$, although the corresponding Schmid factor is very small. The $[0\,1\,0]_{18R}$ is inherited from the $[0\,1\,0]_\beta$ after the β–18R transition. As the 18R–6R transformation was associated with 6R plastic deformation, the yield stress of the 6R martensite was assumed to be less than or equal to the 18R–6R transformation stress.

Although both β ↔ 18R and 18R ↔ 6R martensitic transformations can be easily reverted by removing the load, 6R plastic deformation cannot be reverted. Studies in Cu–Al–Ni shape-memory alloys have shown that, without precipitation treatments, it is possible to induce the 6R phase in adequately oriented single crystals, without permanent deformation after removing the load. Particularly, it was reported that it is possible to avoid plastic deformation for Ni contents higher than 4 wt.%, whilst plastic deformation of the 6R structure takes place during the 18R–6R transition for lower contents of Ni [34,35]. However, Cu–Al–Ni alloys are more brittle and difficult to manufacture [36]. As a result, Cu–Zn–Al alloys can be better choices for certain engineering applications, providing that 6R plastic deformation is controlled.

So, one of the keys to successfully implement the 18R ↔ 6R transformation in engineering applications and profit from its huge hysteresis, large pseudoelastic strain and weak dependence of transformation stresses on working temperature is to isolate this transformation from the plastic deformation of the 6R phase. There are two theoretically possible ways to achieve it: either by increasing the 6R yield stress and/or by reducing the 18R ↔ 6R transformation stress. This study is focused on the former.

The objective of this work is to increase the 6R plastic yield stress by introducing nanoprecipitates into the alloy. This might isolate the 18R ↔ 6R martensitic transformation from the plastic deformation of the 6R phase, allowing for either 18R ↔ 6R or (β–18R–6R) complete mechanical cycles, with little or no plastic deformation. As no information is available on the interaction between the 18R–6R transformation and precipitates, this approach applies the knowledge obtained from the reported results of the interaction between nanoprecipitates and the β–18R phase transformation to the 18R–6R transformation. The effect of introducing γ precipitates on the transformation has been thoroughly analyzed [37–41]. The nanoprecipitates change the chemical composition of the matrix, which in turn changes the equilibrium temperatures between the phases involved and the stress associated with the transformation at a given temperature [41]; however, this is a minor effect for small precipitates. Moreover, nanoprecipitates are expected to interfere with dislocations, disturbing their movement and increasing the yield stresses of all alloy phases [38,42,43]. An interaction between transformation fronts and precipitates might also have an effect

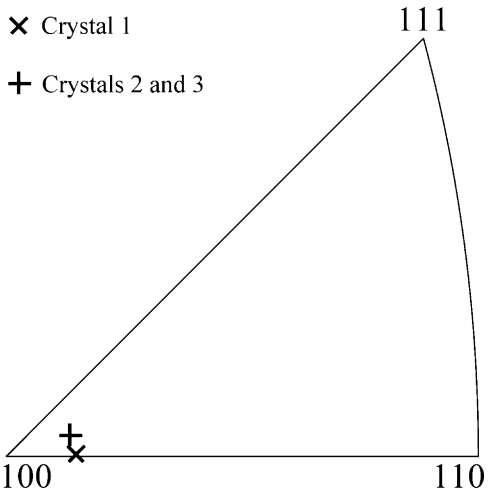


**Fig. 1.** Tensile axis orientation of the crystals used (× corresponds to crystal 1 and + to crystals 2 and 3).

on the hysteresis and transformation stresses, as reported for the β–18R transition [39,40,44].

The present work is focused on the interaction between γ phase nanoprecipitates, the 18R–6R martensitic transition and the movement of dislocations in the 6R structure. Nanoprecipitates are introduced in the β phase by convenient thermal treatments [44]. β phase single crystals with preferred axis orientations are used so that the 6R structure may be induced by tensile stress. The microstructure of the introduced nanoprecipitates is assessed by transmission electron microscopy and the interaction between precipitates and dislocations is analyzed in terms of the Orowan mechanism.

## 2. Experimental procedure

Several Cu–14.78 at%Zn–16.61 at%Al cylindrical single crystals were grown by using the Bridgman method, all with electronic concentration $e/a = 1.48$ and nominal 18R martensitic transformation temperature $M_s = 273$ K. The 18R–6R transformation stress and strain are strongly orientation-dependent, so attention must be paid to the orientation of the crystals used. The minimum 18R–6R transformation stress and its maximum strain are observed when crystals are strained along the $[0\,0\,1]_{BCC}$ direction, which optimizes mechanical properties. However, if the axis is too close to $[0\,0\,1]_{BCC}$, several martensite variants can nucleate, complicating the study of the 18R–6R transformation. In order to minimize the 18R–6R transformation stress and maximize the transformation strain, while avoiding the nucleation of different martensite variants, the orientation chosen for this study is close to, but not exactly, $[1\,0\,0]_{BCC}$.

Crystal 1 was chosen from a group of crystals grown at random (no seed was used). On the other hand, Crystals 2 and 3 were grown from the same seed, so they have the same crystallographic orientation, as shown in Fig. 1. Even though a very small difference in orientation between crystals 2 and 3 might be expected due to the growth method, no measurable difference was detected. Therefore, crystals 2 and 3 are considered to have exactly the same orientation for the purposes of this work. The difference in orientation between crystals 2, 3 and crystal 1 is about 2°. Both orientations chosen maximize the Schmid factor of the 18R–6R transformation, thus minimizing the applied load and reducing the probability of 6R plastic deformation during the transformation or immediately after it.

Cylindrical tensile samples (gage length = 15 mm and diameter = 2.5 mm) were spark machined and then submitted to homogenization at 1103 K in a tubular furnace for 1 h. After homogenization, samples A, C, D and F were air cooled to 796 K and quenched in water at 293 K (thermal treatment TT1). This thermal treatment introduces a dense distribution of γ nanoprecipitates, coherent with the β matrix [44,45]. Samples B and E were immediately quenched from 1103 K in water at 293 K, so that no precipitates are formed (Thermal treatment TT2). The temperature of the samples was monitored with a K-type thermocouple welded to the sample.

**Table 1**
Samples used, with their respective thermal treatments. All samples were submitted to 1-h homogenization at 1103 K and either (a) TT1: air cooled to 796 K and quenched in water at 293 K (precipitation treatment), or (b) TT2: quenched in water at 293 K (no precipitates are introduced).

| Sample | Heat treatment | Precipitates | Crystal | Crosshead speed (mm/min) |
|---|---|---|---|---|
| A | TT1 | Yes | 1 | 0.1 |
| B | TT2 | No | 1 | 0.1 |
| C | TT1 | Yes | 2 | 0.3 |
| D | TT1 | Yes | 2 | 0.3 |
| E | TT2 | No | 2 | 0.3 |
| F | TT1 | Yes | 3 | 0.3 |

After heat treating, all samples were mechanically polished with 600-grit sandpaper and then they were electrochemically polished in a solution of 15% nitric acid in methanol at room temperature, at 10 V.

All samples were tested with an Instron 5567 Machine (or Instron 1123, updated to model 5567). All curves were obtained with an Instron 2620-602 extensometer, unless specifically mentioned. The β-phase initial length is taken as the zero-strain reference in all curves unless otherwise stated.

Latent heat is released – or absorbed – during the transformation or retransformation. Consequently, significant heating – or cooling – of the specimen may take place, depending on the deformation velocity. Hence, crosshead speed was selected so that thermal effects are negligible. To check it, tensile tests were performed at different crosshead speeds. For crosshead speeds equal to or lower than 0.3 mm/min, the β–18R hysteresis remains constant within experimental uncertainties. Thus, a crosshead speed equal to 0.3 mm/min ($3.33 \times 10^{-5}$ s$^{-1}$ in the beginning of the test) was chosen for most of the tensile tests (see Table 1).

In order to isolate the 18R–6R transformation from the β–18R transformation, samples E and F were completely transformed to 18R by tensile stress, at 303 K. Then, under constant load, the temperature was reduced to 253 K, which is below the austenitic start temperature $A_s$. The load was released after cooling and no 18R–β retransformation was observed. The sample was then an 18R single crystal and, as the temperature was kept at 253 K, it was possible to cycle through the 18R–6R transformation without going through the β–18R transformation.

In order to study the microstructure of sample D and calculate its precipitate density, a slice was cut from a region which was not submitted to tensile stresses, perpendicular to the sample axis. The slice was thinned with sandpaper to 0.3 μm and double-jet polished in a Tenupol 3 machine. The electrolyte used was a solution of 500 ml distilled water, 250 ml ethyl alcohol, 250 ml orthophosphoric acid, 50 ml propyl alcohol and 5 g urea. The precipitates were analyzed with a Philips CM200 Ultratwin transmission electron microscope, operating at 200 kV.

## 3. Results

In order to analyze the effects of γ precipitates on the 18R–6R transformations, information on two aspects is required: how the critical stress to obtain the 6R martensite is affected and the effect

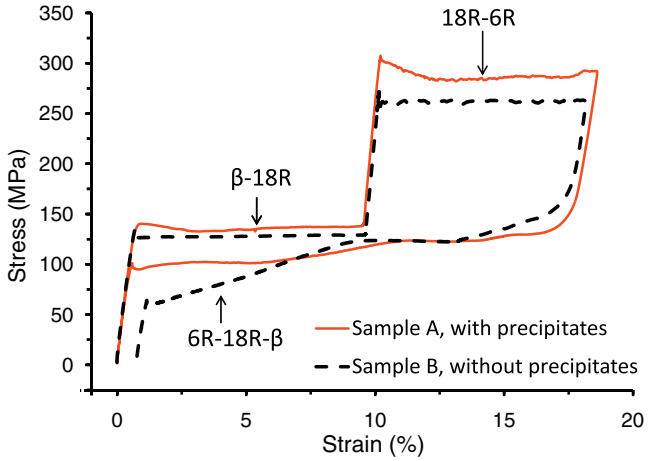


**Fig. 2.** Stress–strain curves for samples A (with precipitates) and B (free of precipitates). The test temperature is 333 K. The martensitic transformations are indicated. Sample A (with precipitates) returns to its original length, whereas sample B (without precipitates) remains longer after the load is removed.

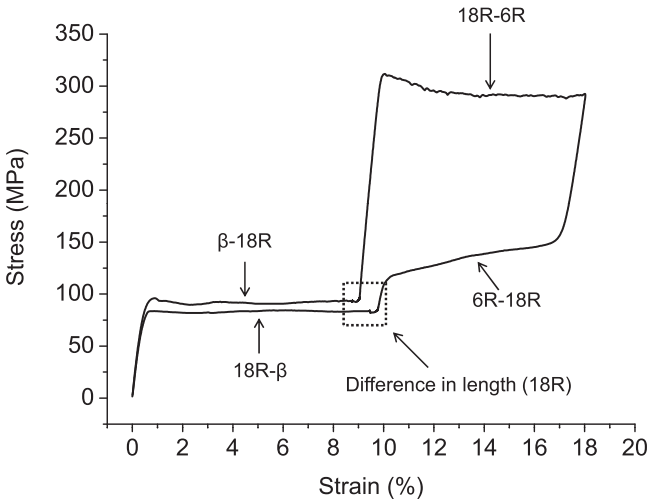


**Fig. 3.** Stress–strain curve, sample A, with precipitates, the test temperature is 303 K. The transformations are shown with arrows and the difference between the length of the sample before 18R–6R transformation and after 6R–18R retransformation is highlighted by the box.

of precipitates on the critical stress to plastically deform the 6R phase. The results of the first point are shown in Fig. 2, where stress–strain curves are presented for samples A and B (with and without precipitates, respectively), tested at 333 K. Sample B was submitted to the same mechanical cycle as sample A, in order to compare the effect of precipitates in the mechanical behavior of samples which are virtually identical, except for the presence of precipitates. This figure clearly shows the following features: (a) no retained deformation is found in sample A, while permanent deformation is observed in sample B, (b) the critical applied stress to obtain 6R martensite, $\sigma^{18R-6R}$, is higher in sample A (a difference of about 20 MPa is measured between the samples) and c) the morphology of the retransformation curve is clearly different for the samples, showing a pronounced slope during part of the retransformation curve in sample B, and a less pronounced effect in the sample with precipitates.

It is interesting to observe here that, although the critical stress to induce the 18R–6R transformation ($\sigma^{18R-6R}$) increases after the introduction of precipitates, no plastic deformation is detected in the material. In order to understand this point, it is necessary to determine the effect of precipitates on the plastic deformation of the 6R structure ($^{6R}\sigma_{pd}$). It is clear from experiments performed in samples without precipitates that plastic deformation takes place during the transformation. As Cuniberti et al. reported the applied transformation stress is the maximum possible value for the plastic deformation of this martensite in samples without precipitates [33].

Sample A was then tested at a lower temperature (303 K). In this case, the β ↔ 18R transformation and retransformation take place at lower stresses, whilst the 18R ↔ 6R transformation stresses change very little. Therefore, both transformations are clearly separated, as shown in Fig. 3. It can be seen that, at the end of the cycle, sample A returns to the same length as before the test, showing no permanent deformation. After the 6*R* → 18*R* path (see the arrow in Fig. 3) the sample is slightly larger than after the β–18R transformation. This fact is tentatively attributed to thin 6R lamellae retained in the 18R martensite, as very thin traces parallel to the common basal plane can be observed in the 18R martensite.

Fig. 4 shows two examples of samples with precipitates which are strained beyond the end of the 18R ↔ 6R transition. Deformation is obtained in sample C from the measured crosshead displacement (Fig. 4a), whereas an extensometer is used with sample D (Fig. 4b), until the onset of 6R plastic behavior. The extensometer was then removed and the sample was strained until fracture, at 29% strain. Both samples belong to the same single crystal, but were tested at different temperatures.

The curves presented in Fig. 4 clearly show the elastic behavior of the 6R structure, which has not been detected in samples without precipitates and, for the first time, a yield stress for the onset of plasticity in this structure can be measured. The values of $\sigma^{18R-6R}$ obtained are 254 and 251 MPa for test temperatures of 303 and 333 K, respectively (stress values were obtained at a strain corresponding to 50% of complete 18R–6R transformation). This slight change fits well with reported data for samples free of precipitates, which show a small negative slope of $\sigma^{18R-6R}$ vs. temperature. The values obtained for $^{6R}\sigma_{pd}$ are 295 and 290 MPa for 303 and 333 K respectively. Considering that $\sigma^{18R-6R}$ is the upper limit of $^{6R}\sigma_{pd}$ in samples free of precipitation, the presence of precipitates increases the plastic yield stress by at least $^{6R}\sigma_{pd} - \sigma^{18R-6R} = 40$ MPa at $T = 333$ K; an increase by approximately the same value is obtained from tests with the same samples at $T = 303$ K. The temperature range is too narrow for us to obtain accurate information on the influence of this parameter on the yield stress of 6R. However, the values obtained are close enough to suggest a slight temperature dependence of this critical stress.

An additional experiment at this stage is presented in Fig. 5: β–18R–6R full cycles with increasing amounts of maximum strain were performed with sample C. No plastic deformation is observed. An interesting point here is that, although the decrease in $\sigma^{18R-6R}$ is noticeable, its consequence to the hysteresis is a reduction of about 9%, an important behavior if potential uses for this transformation are considered. In addition, it should be remarked that pseudoelastic cycles with a total recoverable strain of more than 20% (see also Fig. 4b) are obtained, which may be of interest for some applications.

As mentioned above, γ precipitates do have an influence on the critical stresses to transform from β to 18R and to induce retransformation. A further experiment to decrease a possible overlap of β–18R transformations in the effects reported herein was performed. Single crystals of 18R martensite were obtained by tensile stressing the β phase. These crystals were then cooled down to 253 K under constant load. When the load is removed at this temperature, the specimen remains in the 18R structure, which permits 18R ↔ 6R cycling from null applied stress. Samples E (free of precipitates) and F (with precipitates) were used (details are available in

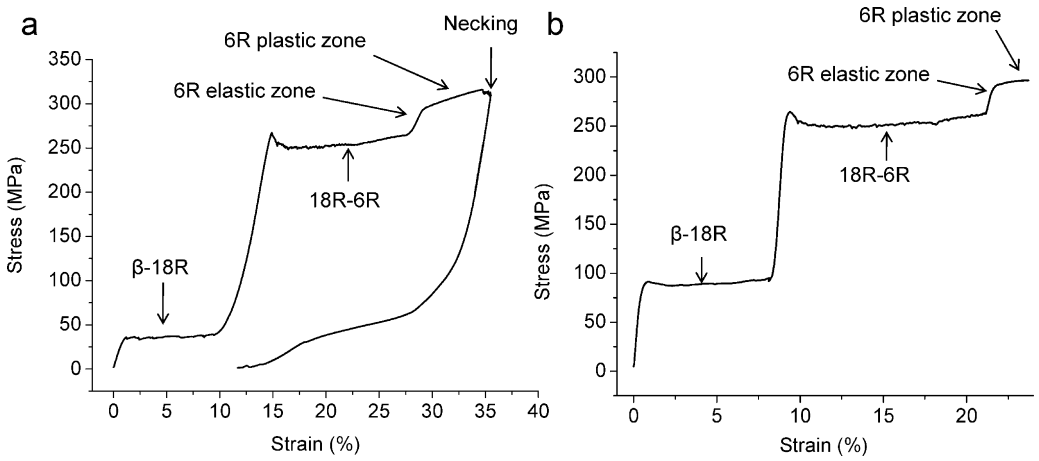


**Fig. 4.** Stress–strain curves for samples C and D (both with precipitates). Complete 18R–6R transitions are obtained. Elastic and plastic deformation of the 6R phase is observed. (a) Sample C, test temperature 303 K, no extensometer was used here, and (b) sample D, test temperature 333 K, an extensometer was used up to 24% strain, which is after the start of the 6R plastic deformation (21.7% strain).

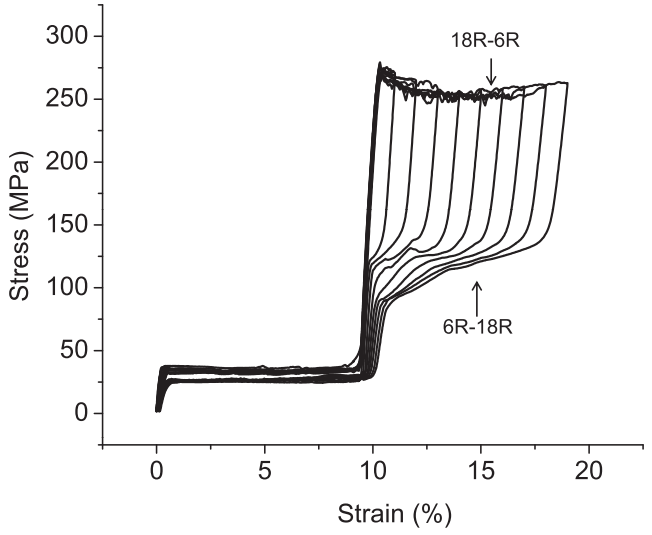


**Fig. 5.** $\sigma$–$\varepsilon$ cycles for sample C, with increasingly higher 6R transformation fraction. The load was completely removed after each cycle, $T_{exp}$ = 303 K.

the Experimental Procedure section). Thus, only one β–18R transformation was induced in each sample. Further cycling between 18R and 6R was performed. The deformation was increased by 0.5% in each cycle. Results are shown in Fig. 6, where the following features can be clearly observed: (a) the retained deformation increases with cycles in sample E, whereas no retained deformation is observed in sample F; (b) no variation in $\sigma^{18R-6R}$ is detected during the cycles performed in sample E while, in sample F, a decrease in this critical stress – about 10 MPa – is observed during the transformation between the first and the second cycles. No further significant reduction in stress is observed in subsequent cycles. At variance with Fig. 2, almost no difference in the 18R–6R transformation stresses between samples E and F is observed in Fig. 6. However, since these specimens belong to different single crystals, small changes in composition might blur the small difference in the stresses observed in Fig. 2.

Sample D was observed in TEM in two-beam condition (Fig. 7). The foil thickness was determined using convergent beam electron diffraction, as shown in the inset in Fig. 7, following the usual procedure [46].

The precipitate density, averaged at three different points, is $\rho = (7 \pm 3) \times 10^{-7}\ \mathrm{nm}^{-3}$. The average precipitate radius is $r = (11 \pm 2)$ nm.

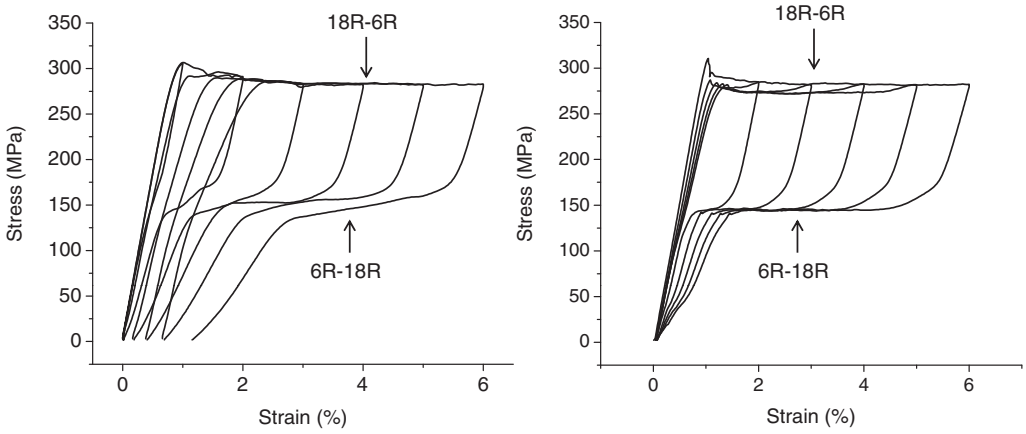


**Fig. 6.** 18R–6R stress–strain cycles at 253 K. The 18R single crystals were obtained by tensile straining the β phase at room temperature and then cooling to 253 K under constant load. Sample E (left), without precipitates, permanent deformation increases in each cycle. Sample F (right), with precipitates, the sample always returns to its initial length, without residual deformation.

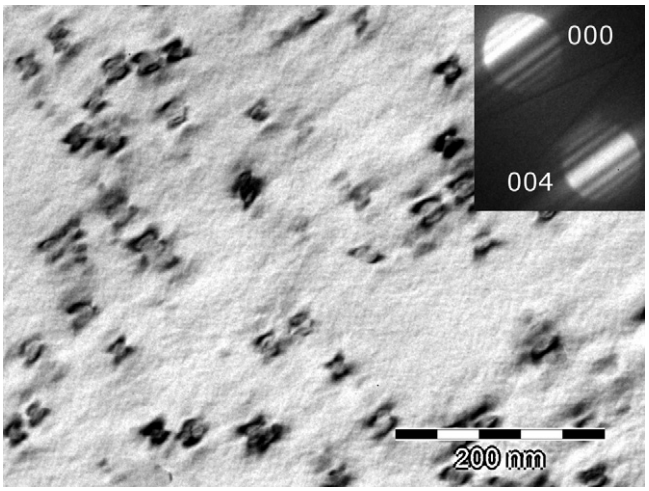


**Fig. 7.** Sample D was observed by TEM in the β phase, under two-beam conditions and zone axis close to $[1\,0\,0]_{\beta}$. Dark zones correspond to the elastic stress field around precipitates. The convergent beam diffraction pattern used to calculate the thickness of the sample is seen on the top right.

The γ phase precipitates are coherent with the β matrix. The line of no contrast perpendicular to 004 diffracting vector can be observed in Fig. 7. The γ phase is an intermetallic compound which is harder than the β matrix and the martensites. Thus the precipitates remain undeformable upon transformation and become incoherent when embedded in the 18R martensitic phase, due to the change of the crystalline structure and the associated shape change of the β matrix [39]. The same behavior is expected for the precipitates in the 6R phase.

Hence, we shall consider that the Orowan mechanism will be the predominant mechanism in the hardening of the 6R phase due to the presence of the small γ phase precipitates.

The increase in the resolved plastic yield stress of the 6R martensite was calculated according to the expression given in [47] that takes into account the various interactions in the Orowan mechanism:

$$\Delta\tau = 0.9\frac{[\ln(8r_s/b)]^{3/2}}{[\ln(L/b)]^{1/2}}\left(\frac{K}{b(L-2r_s)}\right) \quad (1)$$

where $r_s$ is the mean radius of a circular section of the precipitate in any plane and is given in (3), $b$ is the modulus of the Burgers vector, $L$ is the center to center square lattice spacing, given in (4), and $K$ is the prelogarithmic line tension factor for an initially straight edge dislocation in a given anisotropic material. Since the elastic constants of the 6R phase are unknown, we shall consider the isotropic approximation as a first evaluation of the stress hardening. Hence the term $K$ is written as:

$$K = \frac{\mu b^2}{4\pi(1-\nu)} \quad (2)$$

where $\nu$ is the Poisson ratio of the material and $\mu$ is its shear modulus. $r_s$ is defined from the average precipitate radius $r$ as:

$$r_s = \left(\frac{\pi}{4}\right) r \quad (3)$$

and

$$L = r\left(\frac{2\pi}{3f}\right)^{1/2} \quad (4)$$

where $f$ is the volume fraction of precipitates, which can be readily calculated if the shape of precipitates is approximated by spheres:

$$f = \rho\left(\frac{4}{3}\pi r^3\right) \quad (5)$$

The value of the Burgers vector $b$ can be obtained from the lattice parameters of the 6R structure reported by Saule et al. [48] and considering the measured activated slip systems in this phase [33]. A value of $b = 0.262$ nm is obtained.

The elastic constants of the 6R martensite in CuZnAl alloys are not known. However, as a first evaluation, we can make use of the elastic constants of the 18R martensite in this alloy. In order to use the isotropic approximation we could consider the $C_{44}^{18R} = 54$ GPa obtained by Rodriguez et al. [49]. This elastic constant corresponds to a shear deformation on the basal plane along the $[0\,1\,0]_{18R}$ direction, which is a close packed direction. Since the 6R structure inherits the same basal plane, we could assume that the given elastic constant would not change significantly. On the other hand, we can notice that the elastic constants of a Cu–15 at%Zn, solid solution with an FCC structure, are $\mu^{CuZn} = 44$ GPa and $\nu^{CuZn} = 0.308$ for the shear modulus and the Poisson ratio respectively [50]. For α Cu–10 at%Al the elastic constants are $\mu^{CuAl} = 46$ GPa and $\nu^{CuAl} = 0.325$ [50]. As a first approximation we shall take an average value for the shear modulus (including $C_{44}^{18R}$) in (2) as $\mu = 48$ GPa and $\nu = 0.316$ for the Poisson ratio. This gives:

$$\Delta\tau = (28 \pm 11)\,\text{MPa} \quad (6)$$

According to the orientation of the tensile axis used in the present work, a Schmid factor of $\mu_{SF} = 0.4$ is obtained for the normally activated slip systems in the 6R phase, leading to an increase in the applied yield stress of

$$\Delta\sigma = \frac{\Delta\tau}{\mu_{SF}} = (70 \pm 30)\,\text{MPa} \quad (7)$$

This value agrees with the curves in Fig. 4 and allows us to make an estimation of the 6R yield stress without precipitates in sample E: 235 MPa, which is lower than the 18R–6R transformation stress and explains why sample E in Fig. 6 (left) suffers plastic deformation during the 18R–6R transformation, whilst sample F in Fig. 6 (right) is free of plastic deformation.

## 4. Discussion

Precipitates increase the transformation stress and also the hysteresis associated with the β–18R transformation. Moreover, previous studies show that mechanical cycling has an important effect in the hysteresis and transformation stresses in Cu–Zn–Al alloys with nanoprecipitates [39,41]. The magnitude of these effects depends on the size and density of precipitates.

In the present manuscript, a distribution of small-size γ-type precipitates was introduced and it is shown that these precipitates do have a significant effect on the plastic deformation of the 6R phase. A relevant point to be considered is that previous studies and additional experiments performed in this study show that, in samples without precipitates, the 6R martensite deforms plastically while it is being formed [30,33] This fact clearly shows that the critical stress to plastically deform the 6R martensite is lower than the applied stress to obtain this structure, making it difficult to consider potential applications of the 18R–6R phase transformation. The present manuscript presents, for the first time, results which show that a thermal treatment which introduces γ-type precipitates affects, in a different way, the critical stress to induce the 6R martensite and the yield stress to deform this structure plastically. Thus, a complete, reversible cycle is possible, either starting from the β phase and resulting in approximately 20% recoverable deformation or starting from the 18R structure and resulting in about 10% recoverable deformation.

As Fig. 2 shows, the applied critical stress to induce the 18R–6R transition in a sample with γ precipitates, i.e., $\sigma^{18R-6R}$, increased its value by 20 MPa at $T = 333$ K if compared with the material free of precipitates. It has been shown that γ precipitates, depending

on their size, have higher Zn or Al content than the β matrix, leading to a decrease in the electronic concentration of the austenitic structure [41]. According to this and the reported effect of the composition on the equilibrium critical stress, a decrease in the critical stress to obtain 6R should be observed as a consequence of the variation in chemical composition of the matrix [25,27]. It can then be deduced that the increase in $\sigma^{18R-6R}$ comes from the interaction between the transformation front and the precipitates introduced.

A stronger effect is found if the yield stress of the 6R martensite is considered. In order to analyze this point, it is extremely useful to consider that the β phase, having an ordered BCC structure ($L2_1$ type), can be treated as an FCT structure from which the 6R phase could be obtained by an expansion in the $[0\,0\,1]_{BCC}$ direction and a contraction in the $[1\,0\,0]_{BCC}$ and $[0\,1\,0]_{BCC}$ directions. This FCT structure has its $[0\,0\,1]_{FCT}$, $[1\,0\,0]_{FCT}$ and $[0\,1\,0]_{FCT}$ directions parallel to $[0\,0\,1]_{BCC}$, $[1\,1\,0]_{BCC}$ and $[-1\,1\,0]_{BCC}$ respectively. A tetragonal distortion has been introduced as $\psi = (c/a)_{FCT}$, which can in fact be related to the basal plane cell parameters of the martensitic structures, either 18R or 6R phase [27,33,48]. Little information about the mechanical behavior of the 18R–6R transformation in Cu–Zn–Al alloys is available. One study [33] found that, in Cu–Zn–Al single crystals without precipitates, the 18R–6R tensile-induced transformation is accompanied by the plastic deformation of the newly formed 6R phase. In fact, these authors found several activated deformation systems while forming the 6R structure, after testing samples of electronic concentration 1.48 and 1.41. For the sake of comparison, we can consider their findings in samples with $e/a = 1.48$, the same as the present study. They report slip lines corresponding to $\{1\,1\,1\}_{FCT}$ planes and $\langle 1\,1\,0\rangle_{FCT}$ direction, and also traces parallel to the basal plane of 18R phase and $[0\,1\,0]_o$ direction, where the underscored 'o' indicates an orthorhombic index. Assuming that the yield stress of the 6R phase has a maximum value that coincides with the stress to induce the 6R phase, they obtain, for $e/a = 1.48$, a critical resolved shear stress $\leq$114 MPa for slip in $\{1\,1\,1\}_{FCT}\ \langle 1\,1\,0\rangle_{FCT}$ glide system. This particular system was considered because it has the maximum Schmid factor. Considering the orientation they show, the applied stress to transform to 6R in their test was obtained: 270 MPa, very close to the $\sigma^{18R-6R}$ obtained in samples of the present work, with similar tensile axis orientation. The applied stress to plastically deform samples with γ precipitates here obtained reaches at least 290 MPa, sufficiently high to separate transformation and plastic deformation phenomena. Considering the results shown in Fig. 5, the yield stress to deform 6R is higher than the critical stress to induce 6R phase by approx. 40 MPa; in fact, the value also increased if compared with a sample free of precipitates. The precipitates seem to be sufficiently efficient to introduce a hardening effect in the 6R structure, without significantly increasing the 18R–6R transformation stress.

First results on the early cycling stage through the 18R–6R transitions in samples with γ precipitates show that the main change takes place between the first and second cycles, with a decrease in $\sigma^{18R-6R}$. Although microstructural changes are expected to be responsible for this, it is interesting to consider that the corresponding decrease in hysteresis is rather small, (approx. 10%), a fact which encourages further focus on the strategy of introducing γ precipitates to obtain high damping applications.

The Orowan hardening given in expression (7) is consistent with the hardening observed in our mechanical testing. However, due to the various approximations used in its calculation, such value should be regarded as a first estimate of the precipitation hardening of the 6R martensite. In addition to the Orowan mechanisms, other possible phenomena might contribute to the hardening. For example, the small change in matrix composition due to the precipitation and the degree of atomic ordering which depends on the thermal treatment could affect the glide of dislocations in the 6R phase, compared with the precipitate-free phase. However, these contributions are difficult to evaluate and will no be considered in this work.

The 18R–6R transformation in Cu–Zn–Al should be studied thoroughly before its implementation in engineering applications. However, the possibility of inducing partial, or even total, 18R–6R transformation in $e/a = 1.48$ Cu–Zn–Al single crystals, without plastic deformation, leads to a wide new range of options.

## 5. Conclusions

Even though academic interest in CuZnAl shape-memory alloys has decreased in recent years, much remains to be fully understood, particularly the phenomena associated with the 18R ↔ 6R transformation. This study has shown that the 6R plastic yield stress can be increased to about 40 MPa above the 18R ↔ 6R transformation stress by introducing small precipitates of the γ phase. In this way, we have managed to induce the 18R ↔ 6R and the full β–18R–6R martensitic transformation cycles mechanically, with negligible plastic strain, in single crystals of Cu–Zn–Al shape-memory alloys with $e/a = 1.48$. We have also been able to identify elastic behavior in 6R, followed by plastic deformation, necking and fracture, which suggest that the precipitation thermal treatment used is an effective method to isolate the 18R ↔ 6R martensitic transformation from the plastic deformation of the 6R phase. The Orowan mechanism was used to estimate the precipitation hardening. Using several approximations, a hardening of $(70 \pm 30)$ MPa was obtained, which is consistent with the observed hardening with reference to the 18R ↔ 6R transformation stress.

These findings encourage to further investigate the 18R ↔ 6R transformation for specific damping applications or other uses, taking advantage of its good properties, such as large hysteresis (about 150 MPa, applied stress), large recoverable pseudoelastic strain (about 10%) and, particularly, a weak transformation stress dependence on temperature (about −0.42 MPa/K, applied stress).

## Acknowledgments

Argentina (Project PICT 2284-07) and SECTyP UNCUYO – Argentina (Project 06/C321) contributed with financial support. The first author would like to express his gratitude for the doctoral fellowship provided by CONICET-Argentina. Mrs. T. Carrasco helped with the preparation of alloys, Mr. C. Gómez helped with sample preparation, Mr. P. Riquelme provided technical support with testing machines and Mr. R. Stuke improved the system to grow single crystals. We thank Dr. A. Yawny for the fruitful discussions regarding the results in this study.

## References

[1] O. Ben Mekki, F. Auricchio, Int. J. Non-Linear Mech. 46 (2011) 470–477.
[2] V. Torra, A. Isalgue, C. Auguet, G. Carreras, F.C. Lovey, P. Terriault, L. Dieng, Appl. Mech. Mater. 82 (2011) 539–544.
[3] A.M. Sharabash, B.O. Andrawes, Eng. Struct. 31 (2009) 607–616.
[4] S. Casciati, L. Faravelli, Comput. Struct. 86 (2008) 330–339.
[5] Y. Zhang, S. Zhu, J. Eng. Mech. 134 (2008) 240–251.
[6] M.S. Alam, M.A. Youssef, M. Nehdi, Can. J. Civil Eng. 34 (2007) 1075–1086.
[7] V. Torra, A. Isalgue, F. Martorell, P. Terriault, F.C. Lovey, Eng. Struct. 29 (2007) 1889–1902.
[8] C. Auguet, A. Isalgué, F.C. Lovey, F. Martorell, V. Torra, J. Therm. Anal. Calorim. 88 (2007) 537–548.
[9] R. Desroches, B. Smith, J. Earthq. Eng. 8 (2004) 415–429.
[10] M. Ahlers, Prog. Mater. Sci. 30 (1986) 135–186.
[11] R. DesRoches, J. McCormick, M. Delemont, J. Struct. Eng. 130 (2004) 38–46.
[12] A. Yawny, M. Sade, G. Eggeler, Z. Metallkd. 96 (2005) 608–618.
[13] A. Yawny, J. Olbricht, M. Sade, G. Eggeler, Mater. Sci. Eng. A 481–482 (2008) 86–90.
[14] A. Isalgue, V. Torra, A. Yawny, F.C. Lovey, J. Therm. Anal. Calorim. 91 (2008) 991–998.
[15] T. Saburi, in: K. Otsuka, C.M. Wayman (Eds.), Shape Memory Materials, Cambridge University Press, Cambridge, UK, 1998, pp. 49–96.

[16] J. Olbricht, A. Yawny, A.M. Condó, F.C. Lovey, G. Eggeler, Mater. Sci. Eng. A 481–482 (2008) 142–145.
[17] J.F. Beltran, C. Cruz, R. Herrera, O. Moroni, Eng. Struct. 33 (2011) 2910–2918.
[18] S. Montecinos, A. Cuniberti, J. Alloys Compd. 457 (2008) 332–336.
[19] S. Montecinos, A. Cuniberti, A. Sepúlveda, Mater. Charact. 59 (2008) 117–123.
[20] S.H. Chang, Mater. Chem. Phys. 125 (2011) 358–363.
[21] M. Barrado, G.A. López, M.L. Nó, J. San Juan, Mater. Sci. Eng. A 521–522 (2009) 363–367.
[22] U.S. Mallik, V. Sampath, Mater. Sci. Eng. A 478 (2008) 48–55.
[23] A. Baruj, T. Kikuchi, S. Kajiwara, N. Shinya, Mater. Trans. 43 (2002) 585–588.
[24] J.L. Pelegrina, M. Ahlers, Acta Metall. Mater. 40 (1992) 3205–3211.
[25] M. Ahlers, J.L. Pelegrina, Acta Metall. Mater. 40 (1992) 3213–3220.
[26] P. Wollants, J.R. Ross, L. Delaey, Prog. Mater. Sci. 37 (1993) 227–288.
[27] F. Saule, M. Ahlers, Acta Metall. Mater. 43 (1995) 2373–2384.
[28] M. Sade, R. Rapacioli, F.C. Lovey, M. Ahlers, J. Phys. C4–43 (1982) 647–652.
[29] L. Delaey, J. Janssen, J. Van Humbeeck, J. Luyten, A. Deruyttere, Proc. ICOMAT 1979, Cambridge, MA, 1979, pp. 645–648.
[30] G. Barceló, M. Ahlers, R. Rapacioli, Z. Metallkd. 70 (1979) 732–738.
[31] K. Takezawa, T. Izumi, H. Chiba, S. Sato, J. Phys. C4–43 (1982) 819–824.
[32] Z. Saburi, Y. Inada, S. Nenno, N. Hori, J. Phys. C4–43 (1982) 633–638.
[33] A. Cuniberti, R. Romero, Mater. Sci. Eng. A 273–275 (1999) 362–365.
[34] H. Sakamoto, Y. Nakai, K. Shimizu, Trans. JIM 28 (1987) 765–772.
[35] S. Hidekazu, K. Shimizu, Trans. JIM 28 (1987) 715–722.
[36] J. Van Humbeeck, L. Delaey, The Martensitic Transformation in Science and Technology, DGM, 1989, pp. 15–25.
[37] F.C. Lovey, E. Cesari, Mater. Sci. Eng. A 129 (1990) 127–133.
[38] J. Pons, M. Sade, F.C. Lovey, E. Cesari, Mater. Trans. JIM 34 (1993) 888–894.
[39] D. Roqueta, F.C. Lovey, M. Sade, Scripta Mater. 34 (1996) 1747–1752.
[40] D. Roqueta, F.C. Lovey, M. Sade, Scr. Mater. 36 (1997) 385–391.
[41] D. Roqueta, F.C. Lovey, M. Sade, Scr. Mater. 40 (1999) 1359–1365.
[42] M. Sade, C. Damiani, R. Gastien, F.C. Lovey, J. Malarría, A. Yawny, Smart Mater. Struct. 16 (2007) S126–S136.
[43] J. Malarría, F.C. Lovey, M. Sade, Mater. Sci. Eng. A 517 (2009) 118–124.
[44] F.C. Lovey, V. Torra, A. Isalgué, D. Roqueta, M. Sade, Acta Metall. Mater. 42 (1994) 453–460.
[45] F.C. Lovey, R. Rapacioli, M. Chandrasekaran, Phys. Status Solidi A 68 (1981) K105–K111.
[46] D. Williams, C.B. Carter, Transmission Electron Microscopy, II, Diffraction, Plenum Press, New York, 1996, p. 322.
[47] B. Reppich, Materials Science and Technology – A Comprehensive Treatment, vol. 6 – Plastic Deformation and Fracture of Materials, VCH, 1993, pp. 312–355.
[48] F. Saule, M. Ahlers, F. Kropff, E.B. Rivero, Acta Metall. Mater. 40 (1992) 3229–3238.
[49] P.L. Rodriguez, F.C. Lovey, G. Guenin, J.L. Pelegrina, M. Sade, M. Morin, Acta Metall. Mater. 41 (1993) 3307–3310.
[50] P. Robinson, ASM Handbook, vol. 2, Properties and Selection: Nonferrous Alloys and Special-Purpose Materials, ASM, 1990, pp. 917–1150.